Micro and Nano Systems Letters

LETTER Open Access

MEMS particle sensor based on resonant frequency shifting

Ji-Seob Choi and Woo-Tae Park*

Abstract

Recently, as the concentration of fine dust in the atmosphere has increased due to an increase in the use of fossil fuel power plants, automobiles, and factories, it has been increasingly important to measure fine dust in the atmosphere. This is because exposure to fine dust is closely related to the incidence of respiratory and cardiovascular diseases and eventually affects mortality. In this paper, we introduce a MEMS particle sensor based on the resonance frequency shift according to added particle mass. The actuation is driven by Aluminum nitride (AlN), and the total thickness is 2.8 μm. A laser doppler vibrometer (LDV), an optical measuring instrument, was used to measure the resonance frequency of the sensor. Airborne particles naturally were deposited on the sensor. To show the frequency shift according to the particle mass, the frequency shift was measured by dividing the case where the deposited particle mass was small and large. In each case, the frequency shift according to the deposited particle mass was predicted and compared with the frequency shift measured by LDV. It was shown that the deposited particle mass and frequency shift are proportional. The deposition of particulate mass was estimated by image analysis. The frequency shift caused by the particle mass deposited on the sensor was defined as the sensitivity of the sensor. The estimated sensitivity of the sensor is 0.219 to 0.354 kHz/pg.

Keywords: Airborne particle, Microelectron-mechanical-systems (MEMS), Piezoelectric, Particle sensor, Mass sensor, Resonance frequency shift

Introduction

Fine dust is a mixture of solid particles and liquid drops in the air. The exposure to fine dust is closely related to the occurrence of respiratory and cardiovascular diseases and is also reported to increase mortality. Among them, fine dust with a diameter of less than 10 μm can enter the lung and eventually into the blood vessels, which poses a serious threat to human life [1]. Most of these fine dust comes from car exhausts, dust generated during road driving, and also from cigarette smoking and fuel burning [2]. They are mainly composed of combustion particles such as carbon, organic hydrocarbons, nitrates, sulfates, and harmful metals, and because they are so small in size, they can reach deep into the alveoli through the respiratory tract. The smaller the size, the more likely it is to pass through the emphysema directly, allowing for systemic circulation through the blood. Symptoms of such fine dust include coughing and breathing difficulties caused by irritation of the airway during acute exposure, worsening asthma, and arrhythmia. Chronic exposure can reduce lung function and increase chronic bronchitis and, in severe cases, increase mortality [3].

As the risk of exposure to fine dust increases, studies have been conducted to measure the concentration of fine dust in the air such as light scattering method, weight method, and beta rays in order to avoid or prepare for exposure to the fine dust [4, 5]. Optical particle counter is the most popular measurement method in recent years because it is cost-effective, portable, and can be measured in real-time. However, it can only be used at low particle concentrations and has the disadvantage of inferior accuracy when detecting particles smaller than

*Correspondence: wtpark@seoultech.ac.kr
Department of Mechanical Engineering, Seoul National University of Science and Technology, Seoul, South Korea

the wavelength of light. [6]. Another popular method is the Tapered element oscillating microbalance (TEOM). When the particles in the atmosphere are deposited on the device and the mass of the device increases, the vibration frequency decreases. The concentration of the particles in the air is measured by comparing the reduced vibration frequency with the original frequency of the device. The time resolution is short (< 1 h) and has high precision, but there are disadvantages of large volume and high cost [4].

In this study, we developed a high-precision sensor that is cheaper and more portable than an optical particle counter and TEOMs. It is possible to precisely measure the concentration of dust in the air by using frequency shift according to mass change on a micromachined mass, and because it is manufactured by semiconductor process, mass production is possible and product cost can be reduced in high volume [7, 8]. Because it is a MEMS sensor, it has a small size, so it is portable and easy to integrate inside devices and tight space. This particle sensor in this work can be applied to indoor air purifiers, portable dust sensors, clean rooms, and clean benches.

Theory

When the mass of a structure changes, the resonance frequency of the structure also changes. This can be expressed by Eq. (1) [9]

$$F_0^{'} = F_0 \sqrt{\frac{m_{eff}}{m_{eff} + M}} \tag{1}$$

where $F_0^{'}$ is shifted resonance frequency, F_0 is unshifted resonance frequency, m_{eff} is effective mass, and M is added mass. Resonance frequency $F_0^{'}$ decreases by Eq. (1) as the amount of microparticles deposited on the sensor surface increases.

Particle sensor

This particle sensor is composed of 8 layers and its thickness is about 2.8 μm. Table 1 shows the stacking material, stacking order, and thickness of each layer. Figure 1 shows the top view and side view of the stacked layers used in the sensor. As piezoelectric material, AlN was used due to the complete compatibility with other semiconductor processes. AlN has excellent thermal conductivity, excellent electrical insulation, and very close thermal expansion factor to silicon which is used as the main material for semiconductors, so it is highly compatible with silicon [10]. The titanium layer acted as an adhesive layer to form the platinum layer and was formed with a thin thickness. The silicon oxide layer played the role of the insulation layer, while the silicon nitride layer acted as the etching stop layer and a structural layer. The nitride layer is the thickest material along with the piezoelectric layer and makes the piezoelectric layer move away from the neutral plane for piezoelectric movement. The upper and lower electrode pads were formed of gold through a lift-off process and are the two main electrical ports of the device. The membrane shape of the sensor was designed in a circular membrane shape to increase the stiffness than the previously reported beam shape [11]. The diameter was chosen to be 600 μm, which was a balance between particle acceptance area and manufacturing capability. The membrane size beyond 600 um had a low yield in our process run.

Table 1 Thickness of each layer of the particle sensor

No	Material deposited from the bottom	(μm)
8	Silicon dioxide, dielectric layer (SiO_2)	0.2
7	Platinum, top electrode (Pt)	0.2
6	Titanium, adhesion layer (Ti)	< 5 nm
5	Aluminum nitride (AlN)	1.0
4	Platinum, top electrode (Pt)	0.2
3	Titanium, adhesion layer (Ti)	< 5 nm
2	Silicon dioxide, dielectric layer (SiO_2)	0.2
1	Silicon nitride, backside etch stop layer (SiN_x)	1.0

In order to estimate the effective mass of the sensor, the sensor is assumed to consist of the two thickest layers (AlN, SiNx), and the mass is calculated from the volume of each layer and the density of the material. The density value was 3.26 g/cm^3 for AlN and 3.17 g/cm^3 for SiNx, and the mass of the 600 μm circular diaphragm of the sensor was calculated to be approximately 1.818 μg.

Experiment

Figures 2 and 3 are photographs and the block diagram of the measurement setup. The measurement setup consists of an input part, a resonance part, and a measurement part. The input part is a function generator (33500B Series, Keysight INC.), the resonance part is a membrane of a sensor, and a measurement part is an oscilloscope (InfiniVision MSO-X 4154A, Keysight INC.) and the LDV (OFC-2570 controller, OFV-534 header, Polytec INC.). To measure the resonant frequency, we placed the measurement laser point of the LDV at the center of the sensor membrane, where the displacement is the greatest. When the AC signal is applied to the sensor from the function generator, the sensor resonates due to the reverse piezoelectric effect.

The vertical displacement of the center of the resonating sensor is measured at LDV [12] and the output

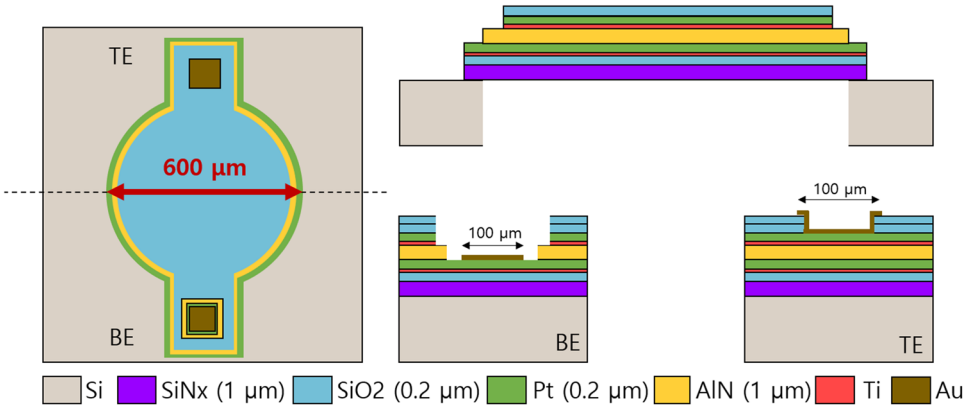

Fig. 1 Top view and side-section of AlN oscillating platform

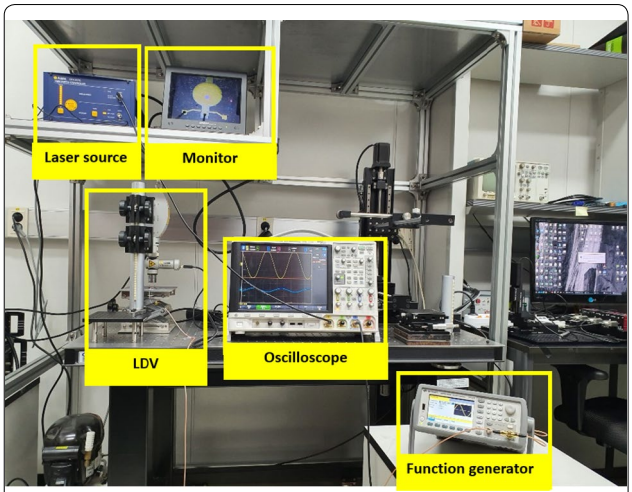

Fig. 2 The setup for measurement of resonance frequency of particle sensor by LDV

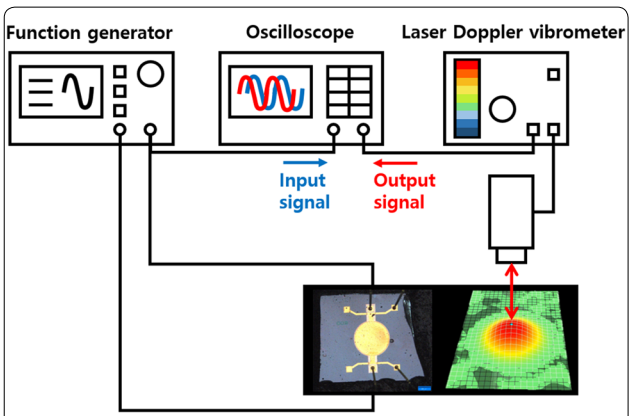

Fig. 3 The block diagram for measurement of resonance frequency of particle sensor by LDV

signal measured at LDV and the input signal from the function generator are simultaneously observed by the oscilloscope. The input voltage is carefully selected so that the displacement at the resonance does not saturate the vibrometer detector sensor. Since the purpose of this experiment is to measure the resonance frequency of the sensor, not the signal strength, the magnitude of the applied voltage is not an important factor. The input signal was applied by manually changing the range from 50 kHz to 3 MHz in 0.1 kHz increments and the output signal was observed with the AC voltage amplitude. Here, the resonance frequency is the point at which the amplitude of the output signal is the maximum in a specific range.

Test particles (A1 ultrafine test dust, ISO-12103-1) used were manufactured by Powder Technology Co., Ltd. from Arizona, USA. The diameter and density of the test dust were 1 to 10 μm, 500 kg/m^3. A simple chamber was manufactured to deposit the fine particles naturally on the sensor surface, and within this chamber, the fine particles diffused slowly and fell on the sensor surface by gravity [11]. All experiments were conducted in a controlled environment. Room temperature was 22 °C and the relative humidity was 50%. To confirm the shift of the resonance frequency according to the particle mass, the particles were deposited on the sensor surface in a small amount case (A) and in large amount case (B) (Fig. 4). Because it is difficult to accurately control the particle mass to be deposited, it was deposited qualitatively. To avoid overlapping of new particles over previously accumulated particles, the sensor surface was forcefully initialized with hand-blower after each resonance frequency measurement. However, some particles were not removed and remained on the surface [13]. This explains why the

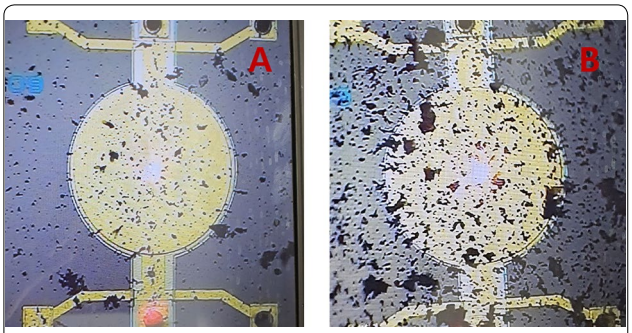

Fig. 4 The airborne particles deposited on the surface of the sensor when there are small amounts of particles (case A) and when there are large amounts of particles (case B)

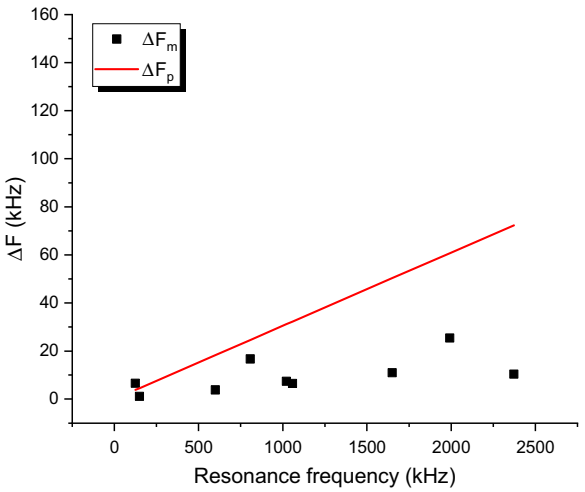

Fig. 5 Resonance frequency shift at each resonance point for case A

resonance points (x-axis) of the sensor in Fig. 6 are not perfectly matched for cases A and B.

Results

Because it is difficult to measure the particle mass deposited on the sensor surface directly [13], the mass of the deposited fine particles was estimated through image analysis through the photo of the sensor surface where the particles were deposited. The program used was ImageJ [14], and it was assumed that the shape of the deposited fine particles is spherical [15]. The volume of each particle could be calculated from the area of the deposited microparticle obtained from the image analysis. The estimated volume of deposited particles in cases A and B of Fig. 4 was 2.32×10^5 μm^3 and 5.02×10^5 μm^3, respectively, with an estimated mass of 116.127 pg and 250.851 pg. Case A represents small amounts of dust particles and case B represents large amounts of dust particles comparatively.

Figure 5 shows the frequency shift data of a single sensor at multiple resonance points for case A (Fig. 4). The x-axis represents the resonant frequencies of the sensor in each mode before particles were deposited, and the y-axis represents the frequency shift. ΔF_m is the measured resonant frequency shift, and ΔF_p is the calculated resonant frequency shift by the estimated particle mass from image analysis. In both ΔF_m and ΔF_p, we can see that the higher the resonant frequency, the higher the resonant frequency shift, which is consistent with the theory [16]. ΔF_m and ΔF_p are not completely in agreement, and this error is expected to have occurred at the resonant frequency measurement and by the random location of the deposited particles on the sensor surface.

There are many factors affecting the accuracy and precision of this experiment. Because we scanned the input frequency manually in 0.1 kHz increment, there may be some resonance point lost between each measurement point. Also, the resolution of the oscilloscope may have been the limitation in finding every resonance point of the sensor in this experiment. Considering the LDV measurement principle of measuring displacement using laser interference, the intensity of the signal can be weakened if particles (obstructions) are present on the laser path of the LDV from the membrane. This can be the explanation why the number of resonance points in A and the number of resonance points in B are not the same. Moreover, this method does not directly measure the resonance frequency shift but measures the resonance frequency before and after the particles are deposited and estimates the frequency shift by pairing similar resonance frequencies among them. In this process, if there are resonance frequencies that are not measured due to small signal strength, an error may occur in the process of calculating the resonance frequency shift. Although it is not the focus in this paper, even if particles of the same mass are deposited, it is expected that the deposition on the center of the membrane affects the vibration more than the same mass deposited at the edge of the membrane. In addition, the mass conversion of deposited particles from image analysis and the resonator-particle adhesion parameter can be a cause of error. The resonator-particle adhesion can be improved by a film coating that increases the adhesion to the membrane [17].

Figure 6 shows the frequency shift at each resonance point when the amounts of deposited particles is small (case A in Fig. 4) and large (case B in Fig. 4). The x-axis represents the resonant frequency of the sensor in each mode before particles are deposited, and the y-axis represents the frequency shift. $\Delta F_{m,A}$ is the shifted resonance

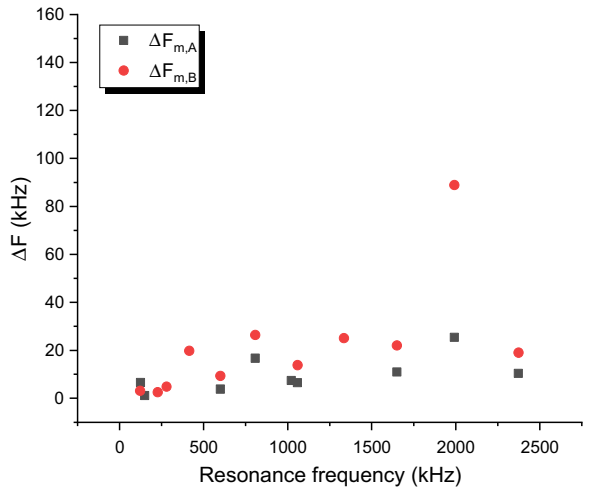

Fig. 6 Comparison of measured resonant frequency shift at each resonance point for case A and B (Fig. 4)

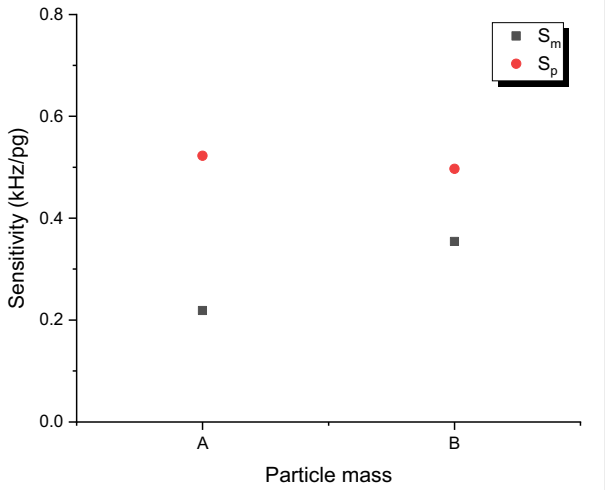

Fig. 7 The sensitivity of the AlN particle sensor according to the particle mass. The discrepancy is due to the assessment of the true particle mass

frequency measured by LDV when the amount of deposited particles is small (case A), and $\Delta F_{m,B}$ is the shifted resonance frequency measured by LDV when the amount of deposited particles is large (case B). Figure 6 shows the tendency that the larger the particle mass deposited, the greater the frequency shift. $\Delta F_{m,A}$ and $\Delta F_{m,B}$ had the largest ΔF at the resonance frequencies of 1991.1 kHz and 1991.9 kHz, and the values were 25.4 kHz and 88.9 kHz, respectively. From Eq. (1) and the resonant frequency of the resonator measured by LDV, we could calculate the mass of the particles deposited on the membrane. The mass data of the deposited particles are 293.208 pg and 562.165 pg, A and B respectively. This was a larger value than the estimated mass of deposited particles through image analysis. The relative errors were 152.488% and 124.103%, respectively. Since most of the particles were naturally deposited in the chamber, it was possible to expect that the measured mass was larger than the estimated mass, because it was more likely to be agglomerated or overlapped rather than a single layer. This is also why the measurement sensitivity (S_m) to be lower than the expected sensitivity (S_p) in Fig. 7.

From Figs. 5 and 6, the sensitivity of the sensor was calculated at the resonance point with the largest ΔF_m. The sensitivity of the sensor is defined as follows [16, 18, 19].

$$S = \frac{\Delta f}{\Delta m} \tag{2}$$

where Δf is the resonant frequency shift, Δm is the estimated deposition mass.

Figure 7 shows the sensitivity of the sensor according to the deposited particle mass in case A and B from Fig. 4. S_m and S_p are sensitivity to the largest frequency shift, ΔF_m and ΔF_p compared to the estimated deposition mass, respectively. S_p was 0.523 kHz/pg and 0.497 kHz/pg for A and B, respectively, and S_m was 0.219 kHz/pg and 0.354 kHz/pg for A and B, respectively.

Conclusion

In this paper, we introduced a MEMS piezoelectric sensor designed to measure fine particles in the atmosphere and used a mass-based resonant frequency shift principle to estimate the mass of particles deposited on the sensor surface. The resonance frequency was measured by LDV, which detects displacement using laser interference. The frequency shift according to the particle mass was confirmed by depositing a small amount of particles and a large amount of particles on the sensor surface, and it was found that the frequency shift increased as the resonance frequency and the deposited particle mass increased. Moreover, the sensitivity was calculated from the frequency shift compared to the estimated mass at the resonance point where the frequency shift was the highest. Reasons for the difference between measurement and calculation could be in the wrong coupling of frequencies in frequency shift and inaccuracies of mass estimation by image analysis. In the future, we plan to use a more accurate test mass, such as glass beads to calibrate the sensor. Also, the sensor will be driven by an oscillator circuit to self-oscillate rather than using a signal generator. Resonant movement should also be measured electrically through a circuit. In the future, we plan to improve the resonance measurement method by measuring the displacement amplitude continuously. The continuous

amplitude measurement can be used to monitor the multiple resonant frequencies more accurately, and the limit of detection (LOD) of the sensor can also be characterized using the quality factor.

Acknowledgements
The authors thank Dr. Byung-Chul Lee for providing the LDV setup and Min-Geon Kim for his contribution in the early stage of this work.

Authors' contributions
WTP supervised the findings of this work and reviewed the manuscript. JSC designed, performed the experiments, and drafted the manuscript. Both authors contributed to the final manuscript. Both authors read and approved the final manuscript.

Funding
This study was conducted with the support industry core technology development program (10070100) of MOTIE (Ministry of Trade, Industry and Energy), Korea.

Availability of data and materials
The datasets supporting the conclusions in this article are included within the article.

Competing interests
The authors declare that they have no competing interests.

Received: 10 July 2020 Accepted: 24 September 2020
Published online: 06 October 2020

References

1. Huang YT, Ghio AJ, Stonehuerner J, Carter JD, Grambow SC, Devlin RB (2003) In ambient fine particles-induced changes. Inhal Toxicol 15:327–342
2. Brocilo D, Podlinski J, Chang S, Mizeraczyk J, Findlay D (2008) Electrode geometry effects on the collection efficiency of submicron and ultra-fine dust particles in spike-plate electrostatic precipitators. J Phys Conf Ser. https://doi.org/10.1088/1742-6596/142/1/012032
3. Udas M (1985) Ultrafine particles. J Jpn Weld Soc. 54(6):318–329. https://doi.org/10.2207/qjjws1943.54.318
4. Amaral SS, de Carvalho JA, Costa MAM, Pinheiro C (2015) An overview of particulate matter measurement instruments. Atmosphere. 6(9):1327–1345. https://doi.org/10.3390/atmos6091327
5. Lee B-J, Park S-S (2019) Evaluation of PM10 and PM2.5 concentrations from online light scattering dust monitors using gravimetric and beta-ray absorption methods. J Korean Soc Atmos Environ. 35(3):357–369. https://doi.org/10.5572/kosae.2019.35.3.357
6. Davitt K et al (2005) 290 and 340 nm UV LED arrays for fluorescence detection from single airborne particles. Opt Express 13(23):9548. https://doi.org/10.1364/opex.13.009548
7. Harrington BP, Abdolvand R, Hajjam A, Wilson JC, Siavash, Thin-film piezoelectric-on-silicon particle mass sensors, 2010 IEEE Int. Freq. Control Symp. FCS 2010, no. July, pp. 238–241, 2010, https://doi.org/10.1109/freq.2010.5556336
8. Hajjam A, Wilson JC, Rahafrooz A, Pourkamali S (2010) Fabrication and characterization of thermally actuated micromechanical resonators for airborne particle mass sensing: II. Device fabrication and characterization. J. Micromech Microeng. https://doi.org/10.1088/0960-1317/20/12/125019
9. Jing BY, Leong KS (2016) Parametric studies on resonance frequency variation for piezoelectric energy harvesting with varying proof mass and cantilever length. J Telecommun Electron Comput Eng. 8(5):119–123
10. Horsley DA et al Piezoelectric micromachined ultrasonic transducers for human-machine interfaces and biometric sensing, 2015 IEEE SENSORS - Proc., pp. 1–4, 2015, https://doi.org/10.1109/icsens.2015.7370564
11. Kim M-G, Choi J-S, Park W-T (2018) MEMS PZT oscillating platform for fine dust particle removal at resonance. Int J Precis Eng Manuf. 19(12):1851–1859. https://doi.org/10.1007/s12541-018-0214-9
12. Huang CH et al Design, modelling, and characterization of display compatible pMUT device, 2018 19th Int Conf Therm Mech Multi-Physics Simul Exp Microelectron Microsystems, EuroSimE 2018, pp 1–4, 2018, https://doi.org/10.1109/eurosime.2018.8369931
13. Ranade MB (1987) Adhesion and removal of fine particles on surfaces. Aerosol Sci Technol 7(2):161–176. https://doi.org/10.1080/02786828708959155
14. Baviskar SN (2011) A quick & automated method for measuring cell area using ImageJ. Am Biol Teach. 73(9):554–556. https://doi.org/10.1525/abt.2011.73.9.9
15. Hamaker HC (1937) The London-van der Waals attraction between spherical particles. Physica 4(10):1058–1072. https://doi.org/10.1016/S0031-8914(37)80203-7
16. Hajjam A, Wilson JC, Pourkamali S (2011) Individual air-borne particle mass measurement using high-frequency micromechanical resonators. IEEE Sens J 11(11):2883–2890. https://doi.org/10.1109/JSEN.2011.2147301
17. A. Improvement and P. Sensors, A simple, low-cost micro-coating method for pressure sensors," pp 1–10, 2019
18. Nazemi H et al (2020) Mass sensors based on capacitive and piezoelectric micromachined ultrasonic transducers—CMUT and PMUT. Sensors. https://doi.org/10.3390/s20072010
19. Pang W, Zhao H, Kim ES, Zhang H, Yu H, Hu X (2012) Piezoelectric microelectromechanical resonant sensors for chemical and biological detection. Lab Chip 12(1):29–44. https://doi.org/10.1039/c1lc20492k

Publisher's Note